



*Anal. Bioanal. Chem. Res., Vol. 7, No. 1, 1-15, January 2020.*

## Electrochemical Sensor for Enantioselective Recognition of Naproxen Using L-Cysteine/Reduced Graphene Oxide Modified Glassy Carbon Electrode

Marzieh Jafari, Javad Tashkhourian\* and Ghodratollah Absalan\*

*Professor Massoumi Laboratory, Department of Chemistry, College of Sciences, Shiraz University, Shiraz 71454, Iran*

*(Received 12 November 2018 Accepted 12 June 2019)*

The electrochemical response of S- and R-naproxen enantiomers were investigated on L-cysteine/reduced graphene oxide modified glassy carbon electrode (L-Cys/RGO/GCE). The production of the reduced graphene oxide and L-cysteine on the surface of the glassy carbon electrode was done by using electrochemical processes. Cyclic voltammetry (CV) and electrochemical impedance spectroscopy (EIS) were used to study the enantioselective interaction between the chiral surface of the electrode and naproxen (NAP) enantiomers. The L-Cys/RGO/GCE was found to be successfully enantioselective toward sensing S-NAP in the presence of R-NAP. The linear dynamic range was found to be  $5.0 \times 10^{-6}$ - $1.3 \times 10^{-4}$  M for both naproxen enantiomers with detection limits of  $3.5 \times 10^{-7}$  and  $2.5 \times 10^{-6}$  M for S- and R-NAP, respectively.

**Keywords:** Chiral recognition, Electrochemical sensor, Reduced graphene oxide, Naproxen, Cysteine

### INTRODUCTION

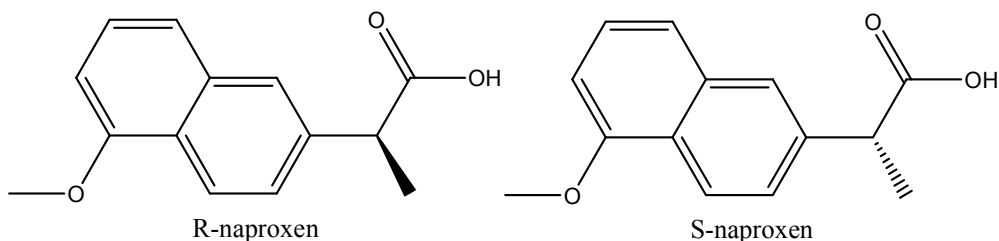
Chiral recognition is the concern of pharmaceutical, chemical and biological studies because the chiral substances are different in bioactivity, pharmacokinetic and metabolic properties in the biological system [1]. There are many available chiral recognition methods including high performance liquid chromatography [2], gas chromatography [3], spectrofluorimetry [4,5], electrophoresis [6], spectrophotometry [7,8], electrochemical methods [9-11]. In chiral compounds recognition, development of simple, sensitive, and efficient assays are highly demanded. In this regard, electrochemical procedures have been found to be promising among the available chiral recognition protocols.

Naproxen (NAP) or naprosyn (Scheme 1) is a nonsteroidal anti-inflammatory analgesic drug which is used in the treatment of many diseases such as osteoarthritis, rheumatoid arthritis, ankylosing spondylitis, juvenile and

rheumatoid arthritis [2]. The pharmacological activity of S-naproxen is 28 times higher than R-naproxen and the naproxen formulations are containing only S-NAP [5,12]. Hence, determination of the composition of naproxen enantiomers is very important in pharmaceutical science. Among the many methods employed to identify the chemical composition of naproxen [2,11-14], electrochemical methods have advantages such as simplicity, low cost, and high sensitivity. Various nanostructure materials have been utilized in electrochemical processes to enhance selectivity and sensitivity of measurements due to the fast electron transfer, electrocatalytic character and large working surface area [15,16].

Graphene, a two-dimensional carbon nanostructure, with high surface area and high intrinsic mobility as well as good electrical conductivity and good dispersivity, is a suitable candidate for detection of biomolecules by using electrochemical methods. Moreover, graphene derivatives with specific functional groups could be potentially useful for these purposes [17]. Recently, nanocomposites based on graphene nanostructures and some biomolecules have been

\*Corresponding authors. E-mail: tashkhourian@susc.ac.ir; absalan@susc.ac.ir



Scheme 1. Chemical structure of naproxen enantiomers

used for fabricating numerous sensors and biosensors [13,17,18]. L-cysteine is an  $\alpha$ -amino acid employed in constructing some nanocomposites for recognition of chiral molecules and drugs [11,18]. In this regard, coating L-cysteine on the surface of an electrode could be useful because introducing different chemical functionalities in this assembly is possible and the system is stable as well [19].

Here, application of glassy carbon electrode, modified by L-cysteine, as a chiral selector, and reduced graphene oxide (L-Cys/RGO/GCE), is demonstrated for enantioselective recognition of NAP enantiomers. Electrochemical technique was applied for the production of reduced graphene oxide and L-cysteine on the surface of a glassy carbon electrode. The chiral recognition was based on different interactions of S- and R-NAP enantiomers with the chiral surface of the constructed enantioselective electrode.

## EXPERIMENTAL

### Reagents

R-naproxen and S-naproxen (purity  $\geq 99\%$ ) were purchased from Merck Company. L-cysteine (purity  $\geq 98\%$ ) was purchased from Fluka Company. To prepare  $1.0 \times 10^{-2}$  M stock solution of R and S-naproxen, an aliquot of 11.5 mg of each enantiomer was individually introduced into a 5-ml volumetric flask and diluted to the mark by deionized water. To prepare the phosphate buffer solution with pH values in the range of 4.0-11.0, a solution of NaOH (0.1 M) was gradually added to a selected volume of  $\text{H}_3\text{PO}_4$  solution until pH meter showed the desired pH value. KCl,  $\text{K}_3[\text{Fe}(\text{CN})_6]$ ,  $\text{K}_4[\text{Fe}(\text{CN})_6]$  salts, and other chemicals such as NaOH and  $\text{H}_3\text{PO}_4$  (85% w/w) were also bought from Merck Company. All chemicals used were of analytical

grade and were used as received without any further purification. Deionized water was used throughout the experiments.

### Apparatus

Electrochemical measurements were carried out with an electrochemical analyzer Autolab PGSTAT 302 N (Metrohm Autolab B.V., Utrecht, the Netherlands). A conventional three-electrode system was used throughout the experiments. The auxiliary electrode was a platinum wire and an Ag/AgCl (3.0 M KCl) electrode was taken as the reference electrode. The working electrode was a glassy carbon electrode (GCE, diameter 2.2 mm) or a modified glassy carbon electrode whichever was required. All experiments were carried out at room temperature in 0.1 M phosphate solution as the supporting electrolyte. Cyclic voltammetric (CV) experiment was performed with a scan rate of  $100 \text{ mV s}^{-1}$  unless otherwise stated. Electrochemical impedance spectroscopy (EIS) and cyclic voltammetry characterization were carried out in a solution of 0.1 M KCl with  $5.0 \times 10^{-3}$  M  $\text{K}_3[\text{Fe}(\text{CN})_6]/\text{K}_4[\text{Fe}(\text{CN})_6]$  as the redox probe. A field emission scanning electron microscopy (FESEM, model Mira 3-XMU) was used for the surface study of the modified electrode. The pH measurements were performed with a Metrohm model 780 pH-meter using a combined glass electrode.

The FTIR spectra were recorded by using an FTIR spectrometer (spectrum RXI, PerkinElmer) equipped with  $\text{CaF}_2$  circular cell windows. The TEM micrographs of the graphene were obtained by a transmission electron microscope (Zeiss, model EL10C) operated at an accelerating voltage of 80 kV. The XRD patterns were acquired by a Bruker D8 Advance X-ray diffractometer using the  $\text{Cu K}\alpha$  radiation line (40 kV, 300 mA) of 0.154 nm and were interpreted by using the X'Pert

HighScore software.

### Synthesis of Graphene Oxide

The modified Hummers method was used for the preparation of graphene oxide from graphite powder [16, 20]. Briefly, 0.5 g of graphite powder, 0.5 g of NaNO<sub>3</sub>, and 23.0 ml of 98% H<sub>2</sub>SO<sub>4</sub> were introduced under stirring into a beaker already placed in an ice bath. Then, 3.0 g of KMnO<sub>4</sub> was slowly added into that beaker while the mixture was thoroughly stirring. Afterward, the beaker was moved into a water bath having a temperature of 35 °C and the solution was stirred for about 1 h to have thick paste. Then, 40.0 ml of deionized water was added to the paste and the mixture was stirred at 90 °C for 15 min. An aliquot of 10.0 ml of 30% (w/w) H<sub>2</sub>O<sub>2</sub> was added to remove the unreacted KMnO<sub>4</sub>. The solid graphene oxide was collected from its suspension by centrifugation at 10000 rpm for 15 min. Then, it was washed with 10% HCl followed by rinsing with deionized water for several times to remove the residual ions as much as possible. A suspension of graphene oxide in water was dialyzed for one week using a dialysis bag with a molecular weight cut off of 8,000 to 14,000 g mol<sup>-1</sup> to completely remove the residual salts and acids [21]. Finally, the product was dried in a vacuum oven at 30 °C for 12 h.

### Preparation of the Modified Electrode

For preparing a graphene oxide-modified glassy carbon electrode (GCE), the surface of a GCE was polished (pretreated) with alumina slurries. Then, it was sonicated, in order, in double distilled water, ethanol, and again in double distilled water for the duration time of 2.0 min for each step. An aliquot of 5.0 µl of water suspended GO (0.2%wt) was cast on the surface of the pretreated GCE. After being dried at room temperature, the GO-modified GCE was immersed into 0.1 M phosphate buffer solution (pH = 7.0), followed by applying a cathodic potential of -0.8 V for 6 min to obtain the reduced graphene oxide (RGO/GCE) [22]. The RGO/GCE was utilized in 10 cycles of cyclic voltammetry (CV) run at a potential range of -0.5 to 2.5 V and at a scan rate of 100 mV s<sup>-1</sup> in the same buffer solution containing 1.0 × 10<sup>-3</sup> M L-cysteine [23]. The fabricated L-Cys/RGO/GCE was rinsed thoroughly with distilled water.

### Electrochemical Measurements

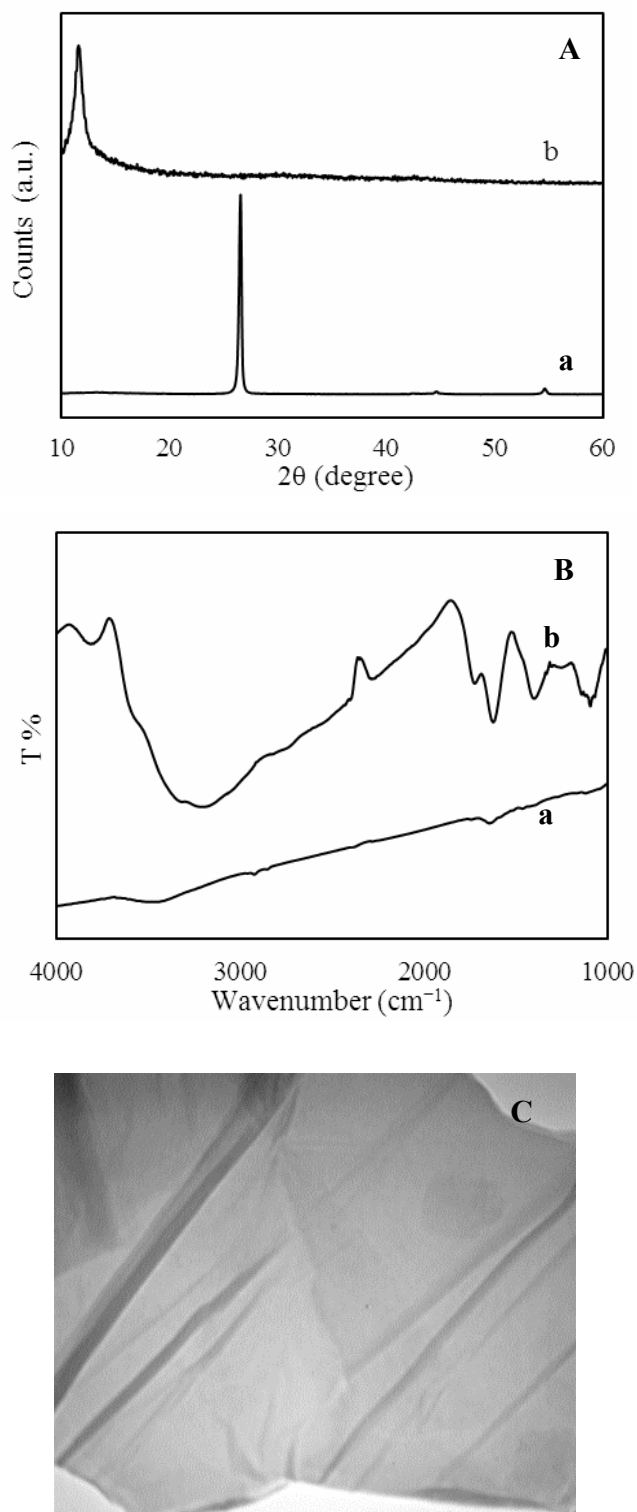
First, the CV of the prepared electrode in 5.0 × 10<sup>-3</sup> M [Fe(CN)<sub>6</sub>]<sup>4-/3-</sup> solution containing 0.1 M KCl was measured. The modified electrode was then immersed into 1.0 × 10<sup>-2</sup> M phosphate buffer solution (pH 6.0) containing 2.0 ml of R- and/or S-naproxen solution (1.0 × 10<sup>-4</sup> M) and CV measurement was performed after 20 min. Finally, the obtained cyclic voltammograms were compared before and after interaction with naproxen enantiomers.

## RESULTS AND DISCUSSION

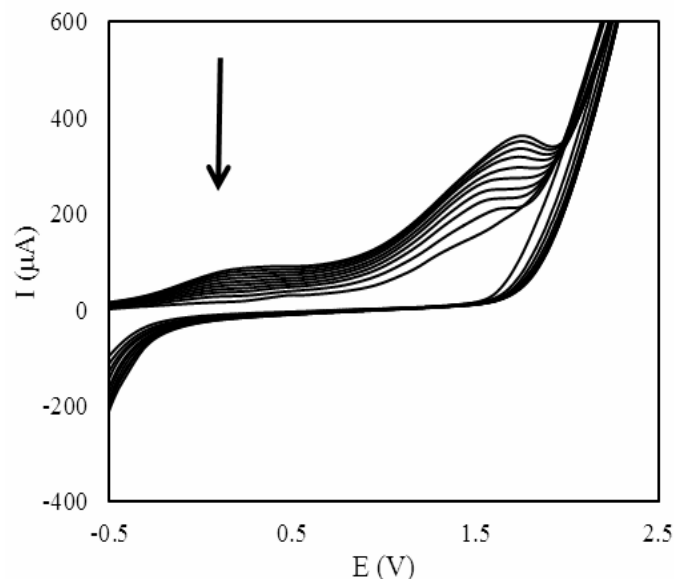
### Characterization of Graphene Oxide

Figure 1A presents the XRD patterns of both graphite and graphene oxide. It should be mentioned that the XRD pattern of the pristine graphite exhibits peaks located at 26.5°, 44.5° and 54.5° corresponding to planes (002), (101), and (004), respectively. The XRD pattern of exfoliated GO illustrated a diffraction peak located at 2θ = 11.6°, corresponding to the (001) interplanar spacing of 0.749 nm [24] which is larger than the interlayer spacing of natural flake graphite (0.34 nm), indicating that oxygen functionalities have facilitated the hydration and exfoliation of GO sheets in aqueous media [25].

The FTIR spectra of both graphite and graphene oxide are shown in Fig. 1B. In the spectrum of graphite, the absorption bands at 3458 cm<sup>-1</sup> belong to the O-H stretching vibration; the peak located at 1634 cm<sup>-1</sup> could be attributed to the skeletal vibration of C=C from unoxidized sp<sup>2</sup> C-C bonds. After performing the oxidation reaction, the FTIR spectra of graphene oxide apparently changed compared to that of graphite. The typical peaks of graphene oxide at 1730 cm<sup>-1</sup> (C=O carboxylic acid and carbonyl group), 3310 cm<sup>-1</sup> (stretching vibration of C-OH) and 1400 cm<sup>-1</sup> (deformation vibration of C-OH) were also observed. The peak at 1060 cm<sup>-1</sup> confirmed the presence of epoxide groups (C-O-C) and the peak at 1630 cm<sup>-1</sup> was ascribed to the skeletal vibration of graphitic skeleton (C=C) [26,27]. To evaluate the morphology of the graphene oxide, transmission electron microscopy (TEM) was performed. Bends and wrinkles on graphene oxide nanosheets at several places (Fig. 1C) are originated by various defects and functional groups carrying sp<sup>3</sup> hybridized carbon atoms introduced during the oxidation process [27]. In general,



**Fig. 1.** (A) The XRD pattern and (B) the FTIR spectra of (a) graphene oxide, and (b) graphite powder, (C) The TEM image of graphene oxide.

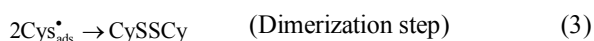
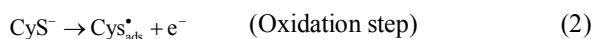
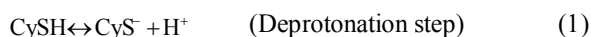


**Fig. 2.** Cyclic voltammograms of RGO/GCE modified by L-Cys. Scan potential, -0.5 to 2.5 V; scan rate, 100 mV s<sup>-1</sup>; pH 7.0 (phosphate buffer solution).

graphene oxide nanosheets tend to assemble with each other and form a multilayer agglomerate [24].

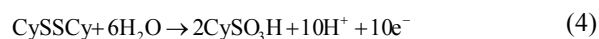
### Modification of the Electrode Using L-cysteine

After modification of the electrode by reduced graphene oxide, it was further modified by using L-cysteine. Figure 2 shows the cyclic voltammograms of L-cysteine electrodeposition on the surface of RGO/GCE. The following oxidation reaction mechanism may occur on the electrode surface [26].



An irreversible oxidation peak (Fig. 2), at *ca.* + 0.3 V, implies that CySH oxidized to L-cystine (CySSCy). Another irreversible oxidation peak was observed at *ca.* + 1.5 V with further scanning. It has been reported that cysteic acid (CySO<sub>3</sub>H) could be found as the oxidation product of CySSCy in many cases [28]. Cystine can be further oxidized to chemisorbing molecules (cysteic acid) at

high positive potential [29,30]:



The SO<sub>3</sub>H functional group of cysteic acid (CySO<sub>3</sub>H) has been confirmed to be strongly adsorbed on the electrode surface [31].

### Characterization of the Modified Electrode

The field emission scanning electron microscope (FESEM) was used for characterization of surface morphology of the modified electrode. The FESEM images of RGO/GCE and L-Cys/RGO/GCE are shown in Fig. 3. As seen in Fig. 3A, RGO on glassy carbon surface illustrates the flake-like shapes of graphene. In Fig. 3B, cysteine molecules deposited on the surface of RGO modified glassy carbon electrode are shown. These results approve the existence of reduced graphene oxide and cysteine on the surface of the modified electrode that is consistent with what have been reported in the literature [18].

### Electrochemical Characterization of the Modified Electrodes

The cyclic voltammetry in ferricyanide was used to

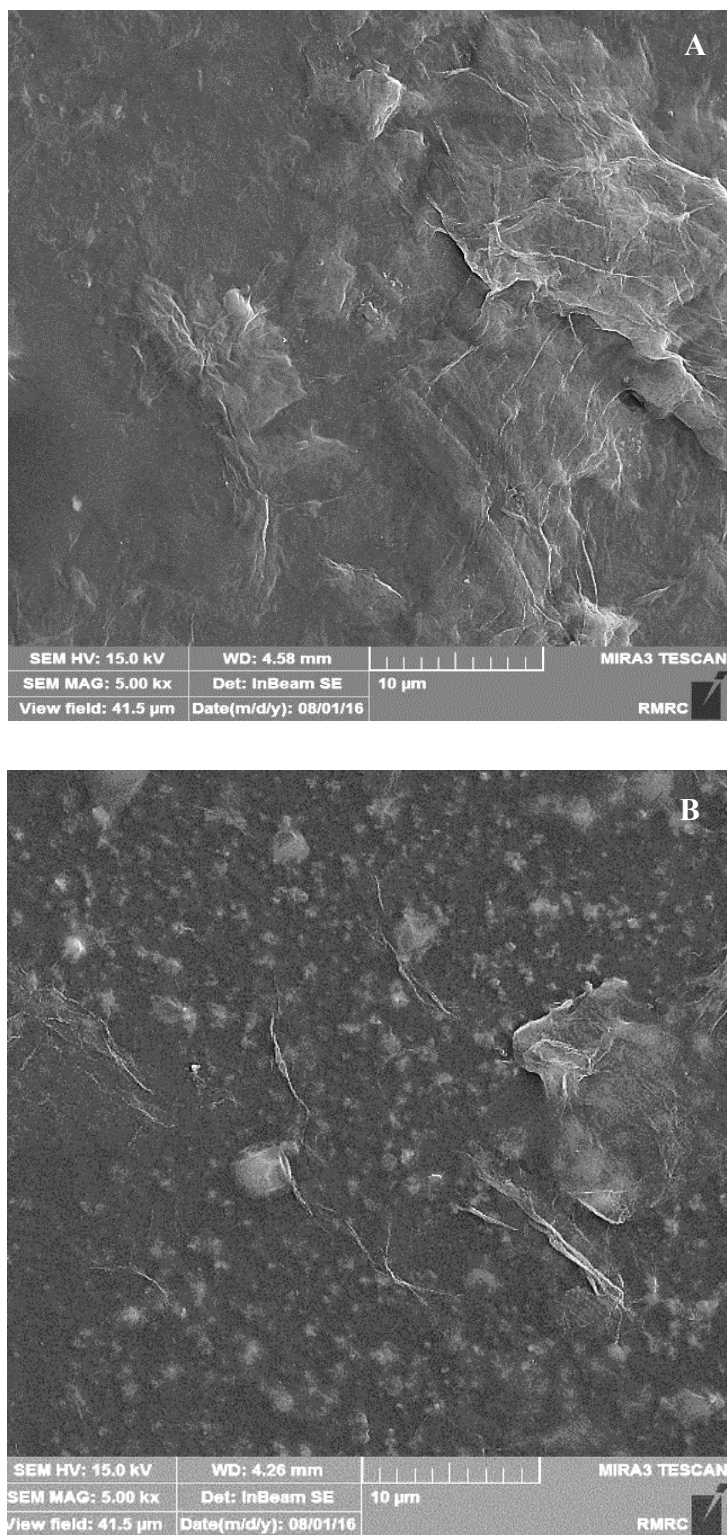


**Fig. 3.** The FESEM images of A) RGO/GCE and B) L-Cys/RGO/GCE.

study the interface properties of the modified electrode. The CVs of different modified electrodes at scan rate of  $100 \text{ mV s}^{-1}$  in  $5.0 \times 10^{-3} \text{ M}$   $[\text{Fe}(\text{CN})_6]^{4-/3-}$  solution containing  $0.1 \text{ M}$  KCl are shown in Fig. 4A. Curve a proves the reversible one-electron redox behavior of  $[\text{Fe}(\text{CN})_6]^{4-/3-}$  ion on the bare glassy carbon electrode. The increase in the electrode surface of the electrode, by electrodeposition of the graphene oxide, could be a reason for the peak current increasing (curve b). By depositing cysteine at the surface of the modified electrode (L-Cys/RGO/GCE), the redox peak current decreased (curve c) and  $\Delta E_p$  increased ( $\Delta E_p = 220 \text{ mV}$ ). This indicated that the deposited layer of cysteine had partially blocked the electron-transfer of  $[\text{Fe}(\text{CN})_6]^{4-/3-}$  at the GCE surface; the results of which was a decrease in the redox current and increase in both oxidation and reduction potentials [11,18,19].

The electrochemical impedance spectroscopy method was used for further characterization of the electrodes. The results are shown in Fig. 4B. A semicircle part, at high frequency region, was displayed by the bare glassy carbon electrode. After modification with graphene oxide, the semicircle diameter of EIS decreased showing that graphene oxide was deposited at the surface of the glassy carbon electrode. After deposition of cysteine, the semicircle diameter increased indicating that cysteine was deposited on the electrode surface. An incomplete semicircle in Nyquist plots, corresponding to a capacitive behavior, was exhibited in this frequency region. It has been argued that the incomplete capacitive semicircle at high frequency region was associated with the L-cysteine layer thickness owing to surface heterogeneity [32-33].

### Determination of the Surface Roughness of the Modified Electrode

The linear relationship between the oxidation peak current ( $I_p$ ) and the square root of the scan rate ( $v^{1/2}$ ) in the range of  $10\text{-}1000 \text{ mV s}^{-1}$ ; obtained based on the CVs of L-Cys/RGO/GCE in  $[\text{Fe}(\text{CN})_6]^{4-/3-}$ , confirmed that the electrochemical process was diffusion controlled (Fig. S1, A). Moreover, the active surface area of L-Cys/RGO/GCE was obtained in  $5.0 \times 10^{-3} \text{ M}$   $[\text{Fe}(\text{CN})_6]^{4-/3-}$  according to the Randles-Sevcik equation [17]. The value of the real surface area for the modified electrode was found to be  $0.1213 \text{ cm}^2$ ; and the value of surface roughness factor

( $R_f = A_{\text{real}}/A_{\text{geom}}$ ) was 3.19 (Fig. S1, B).

Furthermore, the surface coverage of L-Cys/RGO/GCE was compared with bare GCE. For this purpose, the real surface area of GCE was obtained based on Randles-Sevcik equation using  $5.0 \times 10^{-3} \text{ M}$   $[\text{Fe}(\text{CN})_6]^{3-/4-}$  solution at different scan rates. As shown in Fig. S2, the active surface area of glassy carbon electrode was 0.053 and the increase ratio of surface coverage of the modified electrode to non-modified electrode was 2.3.

### Stability and Reproducibility of the Modified Electrode

The stability of the modified electrode was studied by using in  $[\text{Fe}(\text{CN})_6]^{4-/3-}$  at  $100 \text{ mV s}^{-1}$ . After 5 cycles of CV measurement, the relative standard deviation (RSD) of the peak current was 0.89% indicating a good stability of the modified electrode surface. To study reproducibility, construction of the modified electrode was performed five times and the cyclic voltammogram corresponding to each electrode was obtained in  $[\text{Fe}(\text{CN})_6]^{4-/3-}$  solution. The results indicated that the reproducibility was 4.2%.

### Enantioselective Recognition of Naproxen Enantiomers

A procedure for enantioselective recognition of NAP enantiomers was performed by immersing the modified electrode in a solution containing  $5.0 \times 10^{-3} \text{ M}$   $[\text{Fe}(\text{CN})_6]^{4-/3-}$  and  $0.1 \text{ M}$  KCl before (Fig. 5A, a) and after (Fig. 5A, b,c) immersing in  $1.0 \times 10^{-4} \text{ M}$  of either S-NAP or R-NAP solutions for 20 min. A higher decrease in redox peak current (Fig. 5A, c) indicated the presence of an interaction between L-Cys and NAP enantiomers where the interaction with S-NAP was stronger. This showed that the adsorption of S-NAP on the surface of the chiral electrode has provided a superior blocking layer for the electron transfer. The calculated difference between the S-NAP current response change and that of R-NAP,  $\Delta I_{\text{SR}}$  ( $\Delta I_{\text{SR}} = \Delta I_{\text{S}} - \Delta I_{\text{R}}$ ), was  $36.10 \mu\text{A}$ . It should be noted that the change in current response for S-NAP,  $\Delta I_{\text{S}}$  ( $\Delta I_{\text{S}} = I - I_{\text{S}}$ , where  $I$  and  $I_{\text{S}}$  are the peak current before and after submerging the electrode in S-NAP solution, respectively), was found to be  $51.06 \mu\text{A}$ , and the change in the current response for R-NAP solution,  $\Delta I_{\text{R}}$  ( $\Delta I_{\text{R}} = I - I_{\text{R}}$ , where  $I$  and  $I_{\text{R}}$  are the peak current before and after submerging the electrode in R-NAP solution,

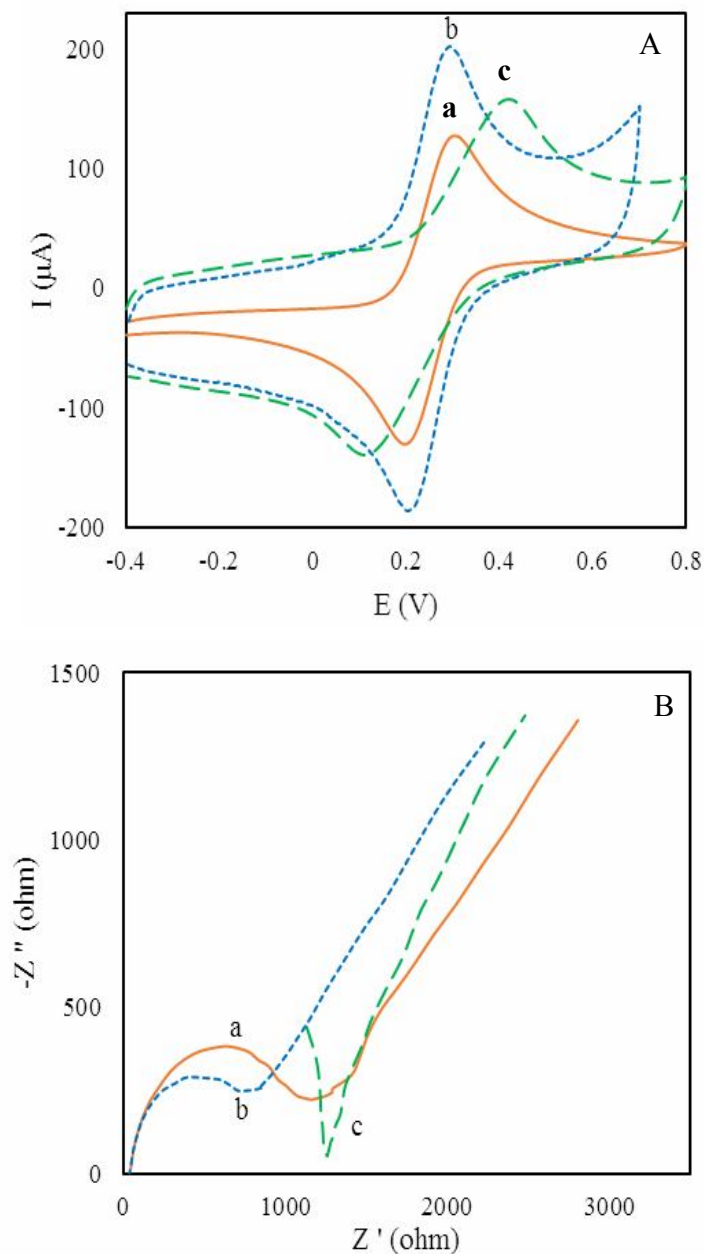


**Fig. 4.** (A) The CV characterization, and (B) the EIS of GCE (a), RGO/GCE (b) and L-Cys/RGO/GCE (c) in  $5.0 \times 10^{-3}$  M  $[\text{Fe}(\text{CN})_6]^{4/3-}$  solution containing 0.1 M KCl. Scan rate was  $100 \text{ mV s}^{-1}$ .

respectively), was found to be  $14.95 \mu\text{A}$ . Thus, the developed chiral sensor was demonstrated to be effective in enantioselective recognition of NAP enantiomers.

The electrochemical impedance spectroscopy (EIS) of the modified electrodes is shown in Fig. 5B, before and

after being immersed in R- or S-NAP solutions for 20 min. After interaction of the modified electrode with R-NAP or S-NAP, the semicircle part of EIS curves increased. It proved that S-NAP had provided higher interaction with electrode surface than R-NAP.

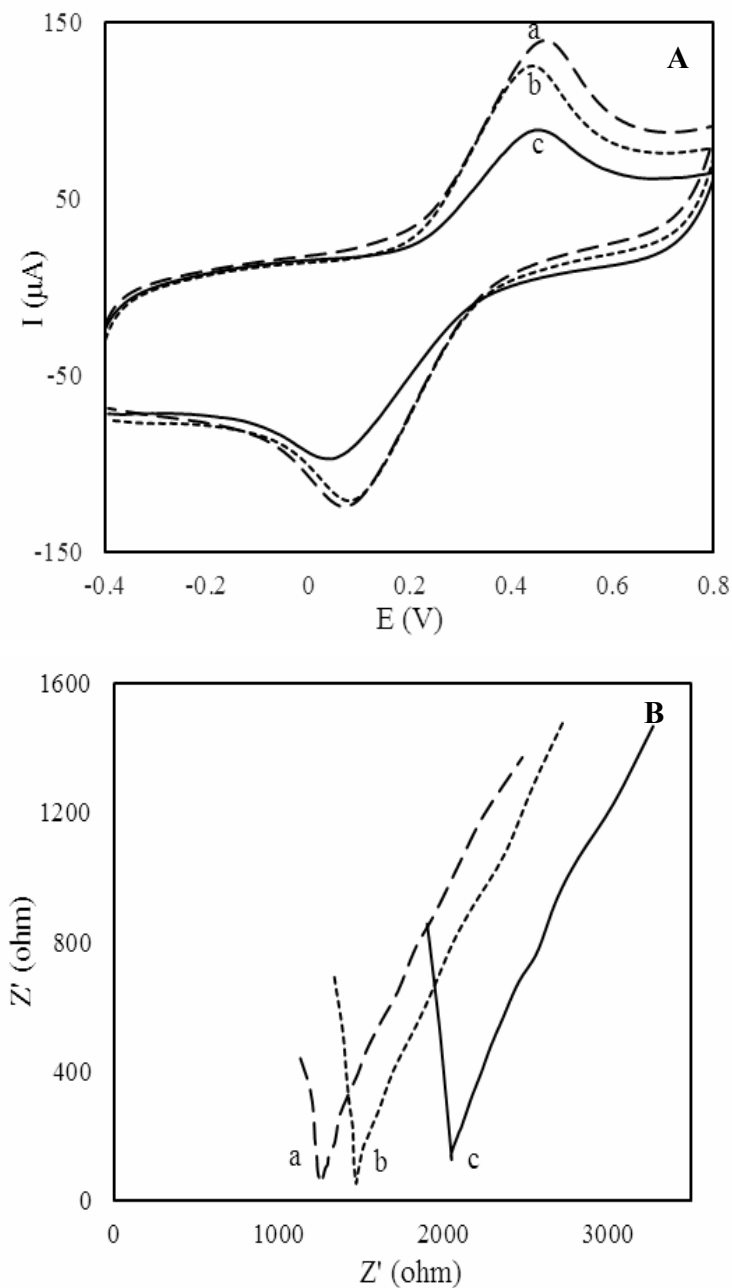


**Fig. 5.** (A) The cyclic voltammograms of  $[\text{Fe}(\text{CN})_6]^{4-/3-}$  at the surface of different electrodes<sup>27</sup>. (B) The EIS of L-Cys/RGO/GCE in  $5.0 \times 10^{-3}$  M  $[\text{Fe}(\text{CN})_6]^{4-/3-}$  solution containing 0.1 M KCl in (a) the absence of NAP, and after interaction with  $1.0 \times 10^{-4}$  M (b) R-NAP and (c) S-NAP.

### Effect of pH and Ionic Strength

To improve the enantiospecificity of NAP enantiomers, the effect of pH on the electrochemical response was

investigated over the pH range of 4.0-11.0 (Fig. 6A). The maximum difference between the peak currents of the enantiomers was observed at pH 6.0 (Fig. 6B). Therefore,

all experiments were performed in pH 6.0. In this pH, cysteine ( $pK_{a1, \text{carboxyl}} = 1.9$ ,  $pK_{a2, \text{amine}} = 8.2$ ) has positive ( $-\text{NH}_3^+$ ) and negative sites ( $-\text{COO}^-$ ), while naproxen

enantiomers has only a negative charge site ( $pK_a = 4.2$ ). Thus, an enantiomer with an appropriate spatial orientation gives effective interaction with L-cysteine, as chiral

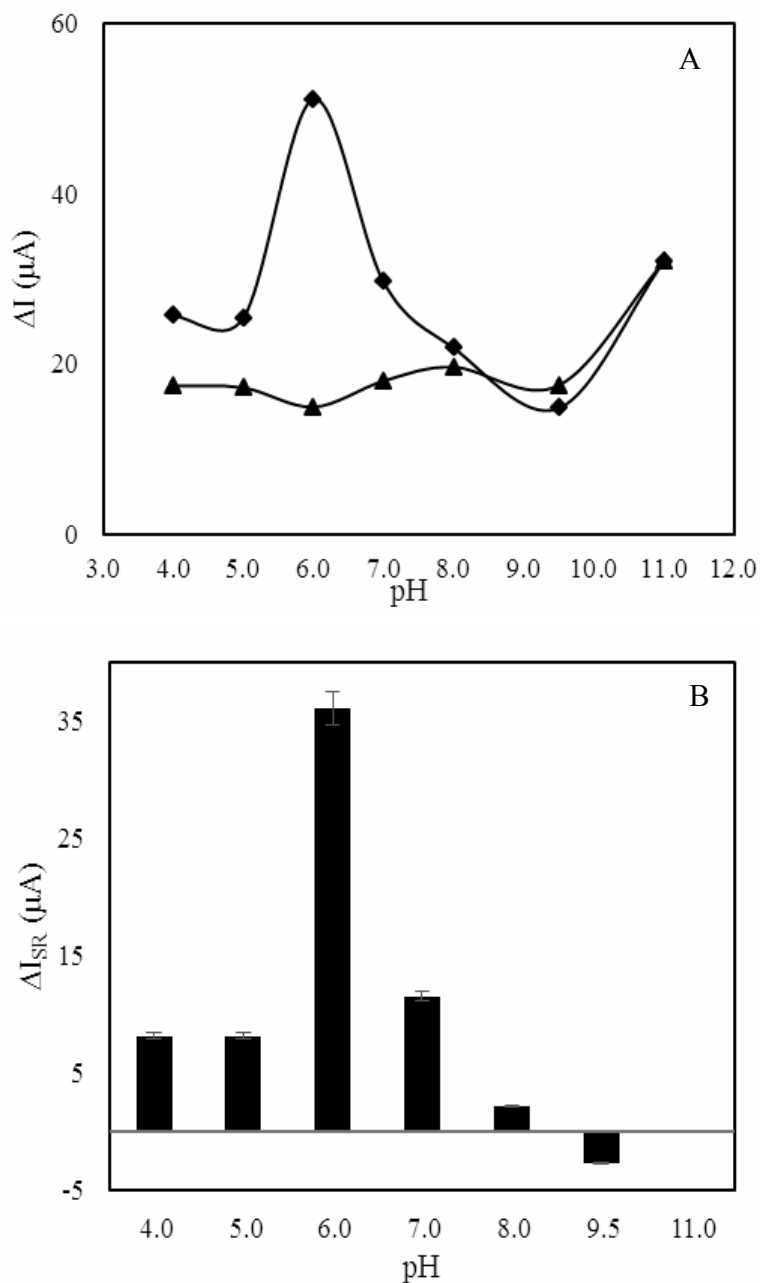


**Fig. 6.** (A) The effect of pH on the peak current change of the chiral sensor for R-NAP ( $\blacktriangle$ ) and S-NAP ( $\blacklozenge$ ) in  $5.0 \times 10^{-3}$  M  $[\text{Fe}(\text{CN})_6]^{4-/3-}$  solution containing 0.1 M KCl. Dependency of pH (B) and ionic strength (C) with  $\Delta I_{SR}$  ( $\Delta I_{SR} = \Delta I_S - \Delta I_R$ ).

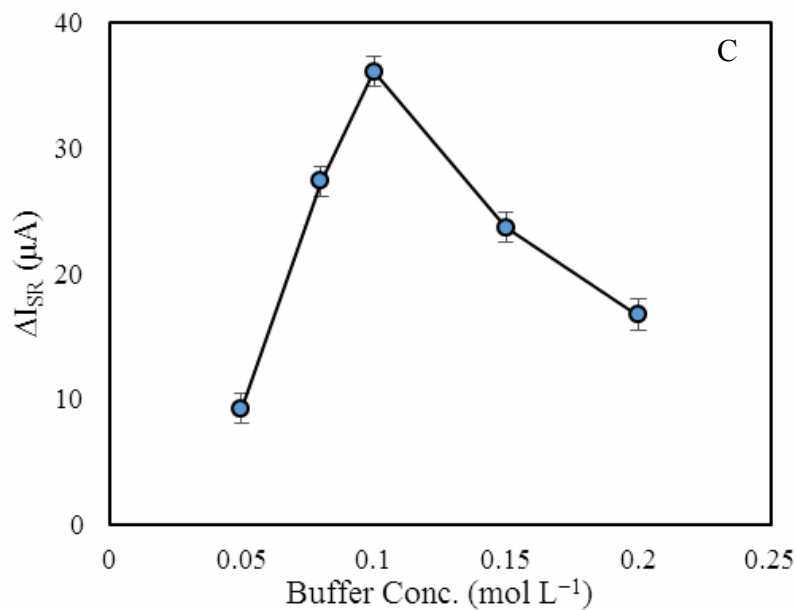


Fig. 6. Continued.

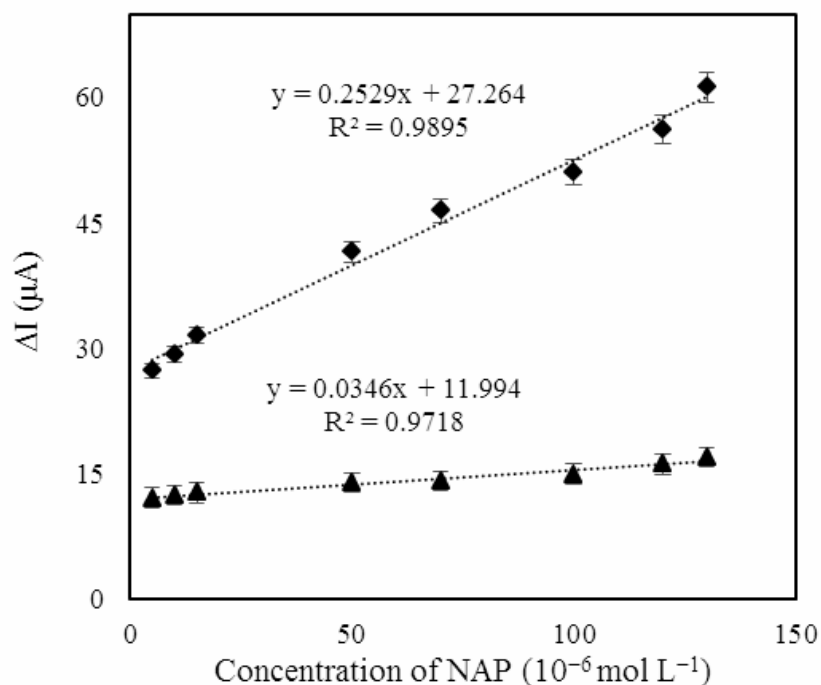


Fig. 7. The relative change of oxidation current peak for R-NAP (▲) and S-NAP (◆) adsorbed on the modified electrode in  $5.0 \times 10^{-3}$  M  $[\text{Fe}(\text{CN})_6]^{4/3-}$  solution containing 0.1 M KCl. Interaction time was 20 min.

selector, on the surface of the electrode.

Effect concentration of phosphate buffer solution was also studied. The results (Fig. 6C) showed that phosphate buffer solution with a concentration of 0.1 M was suitable in chiral recognition of enantiomers. The decrease in interactions of NAP enantiomers with the surface of the modified electrode, as well as decrease in  $\Delta I_{SR}$  with increasing the ionic strength, could be due to inhibiting the interaction of NAP enantiomers with the surface of L-Cys/RGO/GCE by the bulk ions.

### Effect of the Interaction Time

The effect of the interaction time on recognition of NAP enantiomers was investigated from 5.0 to 30.0 min. As Fig. S3 shows, by increasing the interaction time, the difference in peak current change increased. Therefore, 20.0 min was selected as the optimum interaction time value.

### Enantioselectivity Coefficient of the Modified Electrode

Enantioselectivity coefficient ( $\alpha$ ), defined as follows [32], was used to quantitatively evaluate the selectivity of the electrode:

$$\alpha = \Delta I_S / \Delta I_R \quad (7)$$

where  $\alpha$  is the enantioselectivity coefficient (a quantitative measure of a sensor ability to discriminate the S-isomer from the interfering R-isomer);  $\Delta I_S$  and  $\Delta I_R$  are the differences in the anodic peak current after immersion of the modified electrodes, corresponding to the S- and R-naproxen, respectively. The enantioselectivity coefficient of NAP enantiomers was carried out by immersing the modified electrode in a solution containing of  $5.0 \times 10^{-3}$  M  $[\text{Fe}(\text{CN})_6]^{4-3-}$  and 0.1 M KCl at the scan rate of  $100 \text{ mV s}^{-1}$  before and after immersing in  $1.0 \times 10^{-4}$  M S-NAP and R-NAP solutions for 20 min. The enantioselectivity coefficient for the sensor was found to be as 3.4.

### Analytical Parameters

Cyclic voltammograms were obtained in different concentrations of S-NAP and R-NAP. The relationship between the anodic peak current change and the

concentration of each NAP enantiomers (Fig. 7) was linear. Although an increase in the concentration of both enantiomers caused an increase in current change at the L-Cys/RGO/GCE; S-NAP caused a larger current. Therefore, the developed sensor can be used to enantioselectively recognize the NAP enantiomers. The sensitivity of the measurement by the modified electrode was found to be higher for S-NAP than that for R-NAP. The regression equations were  $y = 0.2529x + 27.264$  ( $R^2 = 0.98$ ) and  $y = 0.0346x + 11.994$  ( $R^2 = 0.97$ ) for S- and R-NAP, respectively, where "y" is current differences ( $\Delta I$ ) between NAP enantiomers and "x" refers to S- and R-NAP concentration. The linear range was found to be  $5.0 \times 10^{-6}$ – $1.3 \times 10^{-4}$  M for both NAP enantiomers, and the detection limits (based on  $3\delta/\text{slope}$ ) were obtained as  $3.5 \times 10^{-7}$  and  $2.5 \times 10^{-6}$  M for S- and R-NAP, respectively.

### Application of the Enantioselective Electrode

For studying the application of the chiral sensor, naproxen solutions were prepared with different volume ratios of S-NAP to R-NAP. By increasing the ratio of S-NAP enantiomer to R-NAP, the peak current increased, for both high ( $1.3 \times 10^{-4}$  M) and low ( $5.0 \times 10^{-6}$  M) concentration levels of naproxen (Fig. 8). Moreover, the calibration curves showed good linearity so that the sensor could be used to determine one enantiomer of NAP in the presence of the others.

Also, the developed method was tested for determination of S-NAP in commercial naproxen tablets obtained from Tehrandarou, Sobhandarou and Ruzdarou Compny. For analysis of each drug, ten tablets were accurately weighed and a quantity equivalent to 500.0 mg naproxen from the mixed contents of them was transferred into a volumetric flask. The sample was dissolved in deionized water in alkaline pH. The solution was filtered after 60 minute sonication using an ultrasonic cleaner model CD-4800 (China) at room temperature. Afterwards, 1.0 ml of this solution was diluted to 10.0 ml by adding deionized water where the pH of solution was adjusted to pH = 6.0. Then, the standard addition method was applied for naproxen determination. The results presenting in Table 1 show good recoveries for naproxen tablets.

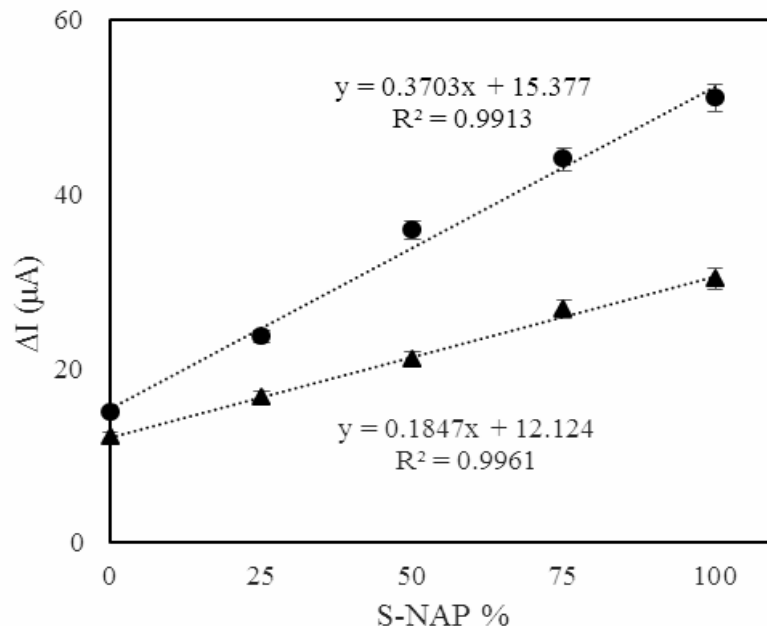


**Fig. 8.** The relative change of the modified electrode oxidation current peak with different enantiomeric compositions of S-naproxen at total NAP concentrations of (●)  $1.0 \times 10^{-4}$  (▲)  $15.0 \times 10^{-6}$  M naproxen.

**Table 1.** Determination of Naproxen in Commercial Naproxen Tablets

Sample	Claimed (mg/tablet)	Found (mg/tablet) ( $\pm$ SD)	Recovery (%)
1	500.0	453.6 $\pm$ 4.8	91.0
2	500.0	484.3 $\pm$ 3.6	96.9
3	500.0	507.2 $\pm$ 5.2	101.4

**Table 2.** Comparison of the Enantioselective Electrochemical Sensors for Naproxen Enantiomers

Type of electrode	Detection method	Linear range (M)	LOD (M)	$\alpha$	Ref.
*TBO/GO/GCE	CV	$5.0 \times 10^{-4}$ - $5.0 \times 10^{-3}$	$3.3 \times 10^{-7}$	2.3	[13]
L-Cys/AuNPs/AuE	CV	$2.0 \times 10^{-6}$ - $2.0 \times 10^{-5}$	$6.7 \times 10^{-7}$	5.4	[11]
L-Cys/RGO/GCE	CV	$5.0 \times 10^{-6}$ - $1.3 \times 10^{-4}$	$3.5 \times 10^{-7}$	3.4	This work

\*TBO: Toluidin blue O.

## CONCLUSIONS

This study shows development of an excellent enantioselective sensor constructed based on L-Cys/RGO/GCE for recognition naproxen enantiomers. The modified electrode could be used successfully for the determination of one naproxen enantiomer in the presence of the others. The linear range was found to be  $5.0 \times 10^{-6}$ - $1.3 \times 10^{-4}$  M for both NAP enantiomers. The detection limits were obtained as  $3.5 \times 10^{-7}$  and  $2.5 \times 10^{-6}$  M for S- and R-NAP, respectively. The electrode showed good stability with relative standard deviation of 0.89%. As Table 2 shows, the obtained enantioselectivity coefficient of 3.4 for the developed sensor is comparable with some sensors reported in this table for determination of naproxen.

## ACKNOWLEDGMENTS

The authors wish to express their gratitude to Shiraz University Research Council for the financial support of this work.

## REFERENCES

- [1] Q. Shen, L. Wang, H. Zhou, H.D. Jiang, L.S. Yu, S. Zeng, *Acta Pharm. Sin. B* 34 (2013) 998.
- [2] S. Corderí, C.R. Vitasari, M. Gramblicka, T. Giard, B. Schuur, *Org. Process Res. Dev.* 20 (2016) 297.
- [3] S.M. Xie, J.H. Zhang, N. Fu, B.J. Wang, L. Chen, L.M. Yuan, *Anal. Chim. Acta* 903 (2016) 156.
- [4] S. Yu, L. Pu, *Adv. Chem.* 2014 (2014) 14.
- [5] P. Damiani, M. Bearzotti, M.A. Cabezón, *J. Pharm. Biomed. Anal.* 29 (2002) 229.
- [6] T. Sohajda, Z. Szakács, L. Szenté, B. Noszál, S. Béni, *Electrophoresis* 33 (2012) 1458.
- [7] Y. Liu, Q. Zhang, Y. Chen, *J. Phys. Chem. B* 111 (2007) 12211.
- [8] M. Zhang, B.C. Ye, *Anal. Chem.* 83 (2011) 1504.
- [9] Z. Li, Z. Mo, S. Meng, H. Gao, X. Niu, R. Guo, *Anal. Methods* 8 (2016) 8134.
- [10] L. Bao, J. Dai, L. Yang, J. Ma, Y. Tao, L. Deng, Y. Kong, *J. Electrochem. Soc.*, 162 (2015) H486.
- [11] A. Afkhami, F. Kafrahi, M. Ahmadi, T. Madrakian, *RSC Adv.* 5 (2015) 58609.
- [12] Y.L. Xu, Z.S. Liu, H.F. Wang, C. Yan, R.Y. Gao, *Electrophoresis* 26 (2005) 804.
- [13] L. Guo, Y. Huang, Q. Zhang, C. Chen, D. Guo, Y. Chen, Y. Fu, *J. Electrochem. Soc.* 161 (2014) B70.
- [14] C. Xiang, G. Liu, S. Kang, X. Guo, B. Yao, W. Weng, Q. Zeng, *J. Chromatogr.* 1218 (2011) 8718.
- [15] D. Saini, R. Chauhan, P.R. Solanki, T. Basu, *ISRN Nanotechnol.* 2012 (2012) Article ID 102543, 12 pages.
- [16] M. Jafari, J. Tashkhourian, G. Absalan, *J. Iran. Chem. Soc.* 14 (2017) 1253.
- [17] W. Feng, C. Liu, S. Lu, C. Zhang, X. Zhu, Y. Liang, J. Nan, *Microchim. Acta* 181 (2014) 501.
- [18] G. Wang, H. Huang, G. Zhang, X. Zhang, B. Fang, L. Wang, *Anal. Methods* 2 (2010) 1692.
- [19] F. Yang, N. Kong, X.A. Conlan, H. Wang, C.J. Barrow, F. Yan, J. Guo, W. Yang, *Electrochim. Acta* 237 (2017) 22.
- [20] W.S. Hummers, R.E. Offeman, *J. Am. Chem. Soc.* 80 (1958) 1339.
- [21] D. Chen, L. Tang, J. Li, *Chem. Soc. Rev.* 39 (2010) 3157.
- [22] S.-J. Li, D. -H. Deng, Q. Shi, S.-R. Liu, *Microchim. Acta* 177 (2012) 325.
- [23] R. Nie, X. Bo, H. Wang, L. Zeng, L. Guo, *Electrochem. Commun.* 27 (2013) 112.
- [24] C. Fu, G. Zhao, H. Zhang, S. Li, *Int. J. Electrochem. Sci.* 8 (2013) 6269.
- [25] Y. Xue, H. Zhao, Z. Wu, X. Li, Y. He, Z. Yuan, *Biosens. Bioelectron.* 29 (2011) 102.
- [26] S. Peng, X. Fan, S. Li, J. Zhang, *J. Chil. Chem. Soc.*, 58 (2013) 2213.
- [27] S. Verma, H.P. Mungse, N. Kumar, S. Choudhary, S.L. Jain, B. Sain, O.P. Khatri, *Chem. Commun.* 47 (2011) 12673.
- [28] W. Chengyin, G. Jun, Q. Qishu, Y. Gongjun, H. Xiaoya, *Comb. Chem. High Throughput Screen.* 10 (2007) 595.
- [29] S. Fei, J. Chen, S. Yao, G. Deng, D. He, Y. Kuang, *Anal. Biochem.* 339 (2005) 29.
- [30] T.R. Ralph, M.L. Hitchman, J.P. Millington, F.C. Walsh, *J. Electroanal. Chem.* 375 (1994) 1.
- [31] N. Spătaru, B.V. Sarada, E. Popa, D.A. Tryk, A. Fujishima, *Anal. Chem.* 73 (2001) 514.

- [32] Q. Cheng, Z. Chen, *Int. J. Electrochem. Sci.* 8 (2013) 8282.
- [33] N. Mahato, M.M. Singh, *Portugaliae Electrochim. Acta* 29 (2011) 233.
- [34] L. Zhang, M. Song, Q. Tian, S. Min, *Sep. Purif. Technol.* 55 (2007) 388.